New aspects of the energetics of ordered Ti_2C and Ti_2N

2007 J. Phys.: Condens. Matter 19 196226

(http://iopscience.iop.org/0953-8984/19/19/196226)

IOP PUBLISHING JOURNAL OF PHYSICS: CONDENSED MATTER

J. Phys.: Condens. Matter **19** (2007) 196226 (22pp) doi:10.1088/0953-8984/19/19/196226

New aspects of the energetics of ordered Ti_2C and Ti_2N

R Eibler

Institut für Physikalische Chemie, Universität Wien, Währinger Straße 42, A-1090 Vienna, Austria

E-mail: renate.eibler@univie.ac.at

Received 22 November 2006, in final form 20 March 2007
Published 26 April 2007
Online at stacks.iop.org/JPhysCM/19/196226

Abstract

Experimentally, two ordered phases of tetragonal symmetry, namely metastable δ'-Ti_2N and stable ϵ-Ti_2N, are found for titanium nitrides of composition Ti_2N, whereas for titanium carbides TiC_x with x near 0.5 two ordered phases with cubic and trigonal symmetry, respectively, can be traced. By experiment, either cubic $Fd3m$-Ti_2C is found to be a metastable phase which transforms at lower temperatures to trigonal $R\bar{3}m$-Ti_2C, or it is detected to be stable for C contents of $0.52 \leqslant x \leqslant 0.55$ and metastable for higher C concentrations of $0.56 \leqslant x \leqslant 0.58$. FP-LMTO calculations confirm the latter and previous FLAPW investigations the former findings.

In the present work, new FLAPW calculations based on the generalized gradient approximation (GGA) for the exchange–correlation potential and using the FLAIR code with force optimization are undertaken for $Fd3m$- and $R\bar{3}m$-Ti_2C, for δ'- and ϵ-Ti_2N and, for comparison, also for the fictitious phases δ'-Ti_2C, ϵ-Ti_2C, $Fd3m$-Ti_2N and $R\bar{3}m$-Ti_2N. These calculations result in cubic $Fd3m$-Ti_2C being the most stable phase and more stable than trigonal $R\bar{3}m$-Ti_2C by 5.0 kJ mol^{-1} at 0 K, provided that the Ti atoms are allowed to relax. For the nitrides, ϵ-Ti_2N is found to be the most stable phase and more stable than δ'-Ti_2N by 3.3 kJ mol^{-1}.

1. Introduction

Transition metal carbides and nitrides are chemically stable, very hard, melt at high temperatures and show a high electric and thermal conductivity. This unique combination of properties makes them highly suitable for various technological applications [1]. They often crystallize in the fcc B1 (NaCl) structure over a wide range of concentration, and their properties are then very sensitive to the concentration and ordering of the structural vacancies on the non-metal sublattice sites.

Regarding the Ti compounds, the cubic δ-phase with the B1 structure and with vacancies statistically distributed on the non-metal sublattice sites can be traced for titanium carbides TiC_x with $0.48 \leqslant x \leqslant 1.0$ [2, 3] and for titanium nitrides TiN_x with $0.42 \leqslant x \leqslant 1.02$ [4–6].

However, by annealing samples with a specific concentration of vacancies, stable ordered defect structures crystallizing in periodic superlattices can be formed [7, 8].

Thus, after annealing TiN_x samples with $0.5 \leqslant x \leqslant 0.6$ at 773 K, ordered, tetragonally distorted δ'-Ti_2N [9–11] is generated. This compound is, however, only metastable [12–14] and transforms by ageing into stable ϵ-Ti_2N crystallizing in the tetragonal antirutile structure [15]. Former FLAPW band-structure calculations also find ϵ-Ti_2N to be more stable than δ'-Ti_2N [16].

For TiC_x ($x \approx 0.5$), on the other hand, two different ordered phases, can be traced, namely cubic $Fd3m$-Ti_2C [17, 18] with 12 atoms per unit cell and trigonal $R\bar{3}m$-Ti_2C [18–20] with three atoms per unit cell. The unit cells of the four ordered defect structures are shown in figure 1.

Experimental investigations disagree about their relative stabilities. At temperatures greater than 700 K, the trigonal phase was found to be stable and the cubic phase metastable for samples of carbon content $0.6 < x < 0.67$, whereas samples with lower C content segregated [7]. By high-resolution electron microscopy, an ordered carbide of composition $TiC_{0.59}$ was identified as $R\bar{3}m$-Ti_2C [21]. Some experiments on samples of a composition near $TiC_{0.6}$ [22, 23] indicate the ordered cubic phase to be stable at higher and the trigonal phase at lower temperatures. For a sample of composition $TiC_{0.62}$, trigonal $R\bar{3}m$-Ti_2C was found to be stable at temperatures below 1053 K [22]. From neutron diffraction studies for samples of composition $TiC_{0.59}$ and $TiC_{0.62}$, it was deduced that the trigonal phase should be stable below 770 K and the cubic phase stable between 770 and 790 K [23]. However, $Fd3m$-Ti_2C also occurs at lower temperatures as a metastable phase because the formation of $R\bar{3}m$-Ti_2C from disordered TiC_x and also from ordered $Fd3m$-Ti_2C is kinetically hindered [22, 23].

Other experiments identify $Fd3m$-Ti_2C as the stable phase for C contents $0.52 \leqslant x \leqslant 0.55$ and $R\bar{3}m$-Ti_2C as stable only for higher C contents of $0.56 \leqslant x \leqslant 0.58$ [24]. Furthermore, transition temperatures from 1000 K [7, 18, 20, 23, 24] to 2000 K [17, 25] are reported in the literature. Due to these experimental uncertainties, the ordered defect structures of Ti_2C are not included in some Ti–C phase diagrams [26].

First-principles calculations also furnish diverging results concerning the relative stabilities of the two Ti_2C phases. In contrast to the present work, a former FLAPW band-structure calculation [27] finds trigonal $R\bar{3}m$-Ti_2C to be more stable than the cubic phase by 34.8 kJ mol^{-1}. On the other hand, an FP-LMTO calculation [28] results in cubic $Fd3m$-Ti_2C with relaxed Ti atoms being more stable than trigonal $R\bar{3}m$-Ti_2C by 1.8 kJ mol^{-1}. However, both full-potential calculations [27, 28] produce quite similar densities of states (DOSs) and also agree in the stabilizing effect of the Ti atom relaxation for the cubic phase.

A calculated phase diagram for the vacancy-ordered structures in substoichiometric TiC_x, established from Monte Carlo simulations, finds the ordered cubic phase to be stable below 1000 K for C contents between $x = 0.5$ and 0.6 and coexisting with the trigonal phase for C contents between $x = 0.6$ and 0.7 [29].

In order to clear up the existing discrepancies for the carbide phases and to find a quantitative explanation for the different stabilities of the respective ordered phases amongst the carbides and the nitrides, new FLAPW [30] calculations were undertaken for $Fd3m$- and $R\bar{3}m$-Ti_2C, for δ'- and ϵ-Ti_2N and, for comparison, also for the fictitious phases δ'-Ti_2C, ϵ-Ti_2C and, for the first time, also for $Fd3m$-Ti_2N and $R\bar{3}m$-Ti_2N. Furthermore, the present work presents some important results not contained in [16], respectively [27], such as the formation energies of the four Ti_2N phases and some electron-density contour plots.

2. Computational aspects

For the present FLAPW calculations, another code than in [16] and in [27], namely the FLAIR code [31], was used. Besides other options, this code offers a choice of different exchange–correlation potentials and also the possibility of calculating the forces acting on the atoms.

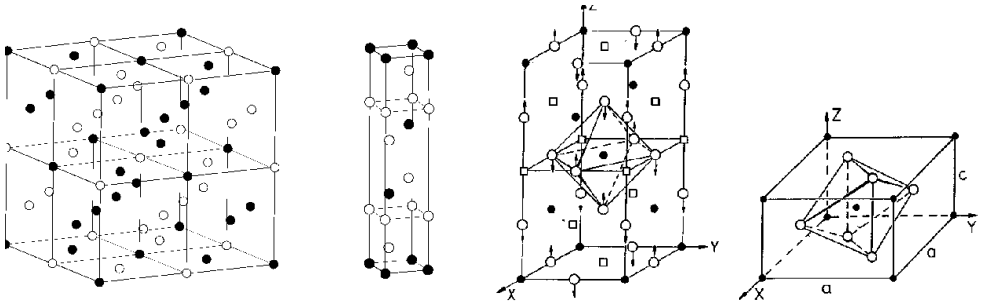

(a) $Fd3m$-Ti_2X (b) $R\bar{3}m$-Ti_2X (c) δ'-Ti_2X (d) ϵ-Ti_2X

Figure 1. Unit cells of the four ordered defect structures (a) $Fd3m$-Ti_2X, (b) $R\bar{3}m$-Ti_2X, (c) δ'-Ti_2X and (d) ϵ-Ti_2X (X = C, N). Full circles, C (N) atoms; empty circles, Ti atoms ($Fd3m$-Ti_2X: vacancies, Ti atoms not shown). The unit cells of $Fd3m$-Ti_2X and δ'-Ti_2X are drawn in a B1 lattice. For $R\bar{3}m$-Ti_2C, one-third of the hexagonal unit cell is shown.

All calculations were performed for a temperature of 0 K and solely for completely ordered phases with the stoichiometric composition $Ti_2C(N)$, corresponding to a C (N) content of $x = 0.5$ for $TiC(N)_x$.

The wavefunctions were expanded into ≈150 so-called augmented plane waves per atom with wavevectors up to $g_{max} = 4.6$ in units of $2\pi/a$. The potential and the electron density were expanded into spherical harmonics up to $l_{max} = 8$ in the muffin-tin spheres around the atomic sites and into a Fourier series up to $K_{max} = 10.0$ (in units of $2\pi/a$) in the interstitial space. For the muffin-tin radii, the same values as in the previous FLAPW calculations [16, 27] were chosen ($r_{Ti} = 1.0577$ Å, $r_{C,N} = 0.9166$ Å).

The Ti 3s and 3p states were treated as core states with a correction for the tails of the corresponding atomic wavefunctions extending outside the muffin-tin spheres. Using the FLAIR code, it is no longer necessary to give the energy parameters of the Ti s and p states fixed values in order to avoid the occurrence of ghost bands as had to be done in the former FLAPW calculations [16, 27]. Therefore, in the present work all energy parameters including the Ti 3s and 3p parameters were determined from the centre of gravity of the corresponding l-like energy bands of the previous iteration. All core states were treated fully relativistically.

For all Ti_2N and Ti_2C phases, GGA (generalized gradient approximation) band-structure calculations with a PW91 exchange–correlation potential [32] were performed.

In all structures, the Ti atoms were allowed to relax. For each geometry, the relaxations and energy minima were determined by calculating and optimizing the forces acting on the atoms.

The equilibrium geometries and total energy minima for either relaxed or unrelaxed Ti atoms were determined by Birch fits [33] to the total energies calculated at various volumes. For the trigonal and tetragonal structures, the c/a ratios were also optimized.

For the integration in $\vec{k}$ space, Fermi-broadened one-electron energy states were calculated at 72 ($Fd3m$-Ti_2C (Ti_2N)), 288 (both $R\bar{3}m$-Ti_2C (Ti_2N) and ϵ-Ti_2C (Ti_2N)) and 244 (δ'-Ti_2C (Ti_2N)) $\vec{k}$ points in the irreducible wedges of the respective Brillouin zones. These $\vec{k}$ meshes were regarded to be sufficiently large because the total energies did not change significantly when energy states at a higher number of $\vec{k}$ points were taken into account. A Fermi-function broadening of 0.003 eV was used throughout.

In order to enable the comparison with thermodynamic data, the formation energies per atom E_{form} were calculated for the carbide phases by

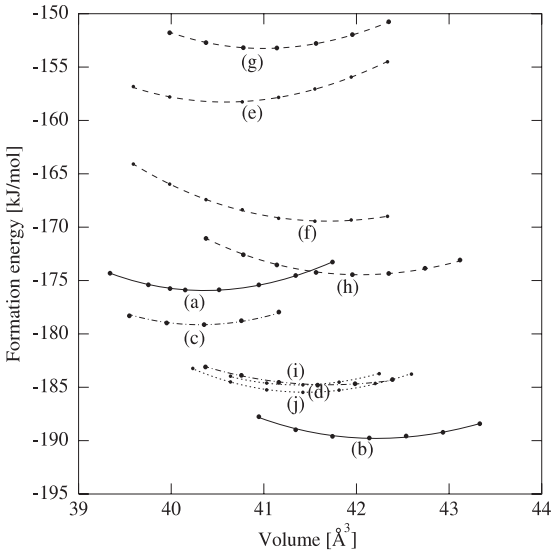

Figure 2. Formation energies (in kJ mol^{-1} of Ti_2C) of various ordered titanium carbide phases of composition Ti_2C resulting from GGA-PW91 band-structure calculations: (a) unrelaxed $Fd3m$-Ti_2C; (b) relaxed $Fd3m$-Ti_2C; (c) unrelaxed $R\bar{3}m$-Ti_2C, optimized c/a ratio (4.6259); (d) relaxed $R\bar{3}m$-Ti_2C, optimized c/a ratio (4.7232); (e) unrelaxed δ'-Ti_2C, $c/a = 2.0$; (f) relaxed δ'-Ti_2C, $c/a = 2.0$; (g) unrelaxed δ'-Ti_2C, $c/a = 2.1$; (h) relaxed δ'-Ti_2C, optimized c/a ratio (2.1); (i) unrelaxed ϵ-Ti_2C, optimized c/a ratio (0.62034); (j) relaxed ϵ-Ti_2C, optimized c/a ratio (0.62648).

$$E_{\text{form}} = \frac{E(\text{Ti}_m\text{C}_n) - mE(\text{Ti}_{\text{hcp}}) - nE(\text{C}_{\text{Graphite}})}{n+m} \tag{1}$$

and for the nitride phases by

$$E_{\text{form}} = \frac{E(\text{Ti}_m\text{N}_n) - mE(\text{Ti}_{\text{hcp}}) - nE(\text{N}_{2(\text{g})})}{n+m}. \tag{2}$$

3. Results

3.1. Ti_2C phases

3.1.1. Energetics. Figure 2 shows the volume dependence of the formation energies of unrelaxed and relaxed $Fd3m$-Ti_2C, of unrelaxed and relaxed $R\bar{3}m$-Ti_2C with the optimized c/a ratio, respectively, of fictitious unrelaxed and relaxed δ'-Ti_2C with $c/a = 2.0$ and $c/a = 2.1$, respectively, and of fictitious unrelaxed and relaxed ϵ-Ti_2C with the optimized c/a ratio, respectively. The plots are based on GGA band-structure calculations with the PW91 exchange–correlation potential [32].

In opposition to [27] but in agreement with [28], relaxed $Fd3m$-Ti_2C is found to be the most stable phase. The least stable structure turns out to be unrelaxed δ'-Ti_2C.

The differences in the energetics resulting from the present work and the former FLAPW calculation [27] can be ascribed to now using a newer, more reliable code, to determining the equilibrium geometries by force optimization instead of simply minimizing the total energy and to using a different approximation for the exchange–correlation potential (GGA-PW91 instead of LDA-HL [34]).

Table 1. Relaxation of Ti atoms in $Fd3m$-Ti_2C, $R\bar{3}m$-Ti_2C, δ'-Ti_2C and ϵ-Ti_2C.

Method	Relaxation (Å)	Relaxation energy (kJ mol^{-1})	Volume increase (%)
		$Fd3m$-Ti_2C	
GGA/FLAPW	0.038	−13.9	4.6
LDA/FLAPW [27]	0.038	−8.4	2.3
LDA/FP-LMTO [28]	0.080	−11.7	3.0
GGA/VASP [38]	0.054	—	—
exp. [17]	0.040	—	—
		$R\bar{3}m$-Ti_2C	
GGA/FLAPW			
$c/a = 4.7232$	0.038	−6.6	3.5
GGA/VASP [38]			
$c/a = 4.6832$	0.064	—	—
		δ'-Ti_2C	
GGA/FLAPW			
$c/a = 2.0$	0.067	−11.2	2.7
$c/a = 2.1$	0.105	−21.2	2.5
		ϵ-Ti_2C	
GGA/FLAPW			
$c/a = 0.6265$	0.008	−0.8	0.3

Unrelaxed trigonal $R\bar{3}m$-Ti_2C is stabilized by a distortion reducing the experimental c/a ratio by 5%. When the Ti atoms are allowed to relax, the optimized c/a ratio rises to 4.7232 (still 3% below the experimental value), but even then trigonal $R\bar{3}m$-Ti_2C at the corresponding equilibrium volume is less stable by 5 kJ mol^{-1} than relaxed cubic $Fd3m$-Ti_2C.

For all phases, the Ti atoms are found to relax (see also table 1). For $Fd3m$-Ti_2C and δ'-Ti_2C, the relaxations of the Ti atoms refer to the ideal positions of the fcc sublattice, for $R\bar{3}m$-Ti_2C to their experimental atomic coordinates and for fictitious ϵ-Ti_2C to the experimental coordinates of the Ti atoms in ϵ-Ti_2N. The relaxation of the Ti atoms reduces the nearest-neighbour Ti–C distance and lowers the total energy. The calculated relaxation for $Fd3m$-Ti_2C agrees well with the experimental value [17].

The stabilizing effect of relaxation becomes more important with increasing volume. Therefore, the calculated equilibrium volumes of the relaxed carbides are larger than the equilibrium volumes of the unrelaxed carbides.

Relaxation and relaxation energy are largest for δ'-Ti_2C. They increase with the c/a ratio.

In table 2, the equilibrium geometries, bulk moduli and formation energies (in kJ Mol^{-1}) for different Ti_2C phases resulting from the present GGA-FLAPW band-structure calculations are shown together with various calculated and experimental values from the literature and especially with results for $Fd3m$- and $R\bar{3}m$-Ti_2C from recent VASP calculations [38].

In order to be comparable with the FLAPW results, the VASP calculations were also performed assuming the Ti 3p states to be core states.

Both calculations predict relaxed $Fd3m$-Ti_2C to be more stable than trigonal $R\bar{3}m$-Ti_2C and find a reduction of the equilibrium c/a ratio of $R\bar{3}m$-Ti_2C with respect to the experimental value, but the equilibrium lattice parameters of the GGA/FLAPW calculation with relaxed Ti

Table 2. Equilibrium lattice parameters (in Å), compression moduli B_0 (in GPa) and formation energies (in kJ mol^{-1}) of various ordered titanium-carbide phases with unrelaxed and relaxed Ti atoms.

	Unrelaxed Ti				Relaxed Ti			
Method	a	c	B_0	E_{form}	a	c	B_0	E_{form}
				$Fd3m$-Ti_2C				
GGA/FLAPW	8.64	—	200	−176.0	8.77	—	163	−189.8
LDA/FLAPW [27]	8.49	—	208	−200.1	8.55	—	207	−208.3
LDA/FP-LMTO [28]	8.41	—	213	−183.9	8.50	—	204	−195.7
GGA/FP-LMTO [37]	8.54	—	177	—	—	—	—	—
LDA/VASP [38]	—	—	—	—	8.48	—	—	−190.2
GGA/VASP [38]	—	—	—	—	8.64	—	—	−192.2
exp.	—	—	—	—	8.60	—	178	−195.7[a] [39]
	—	—	—	—	[17]	—	[37]	−192.2[a] [40]
				$R\bar{3}m$-Ti_2C				
GGA/FLAPW								
$c/a = 4.6259$	3.11	14.39	211	−179.2	—	—	—	—
$c/a = 4.7232$	—	—	—	—	3.13	14.78	126	−184.7
LDA/FLAPW [27]								
$c/a = 4.6259$	3.05	14.13	211	−243.0	—	—	—	—
LDA/FP-LMTO [28]								
$c/a = 4.8956$	2.97	14.54	—	−193.4	—	—	—	—
LDA/VASP [38]								
$c/a = 4.6713$	—	—	—	—	3.03	14.15	—	−188.6
GGA/VASP [38]								
$c/a = 4.6832$	—	—	—	—	3.09	14.45	—	−190.3
exp.:								
$c/a = 4.8694$ [7]	3.06	14.91	—	—	—	—	—	—
				δ'-Ti_2C				
GGA/FLAPW								
$c/a = 2.0$	4.33	8.66	179	−158.2	4.37	8.74	154	−169.3
$c/a = 2.1$	4.27	8.98	194	−153.2	4.31	9.05	161	−174.5
LDA/FLAPW [27]								
$c/a = 2.0$	4.25	8.50	212	−220.5	4.28	8.56	216	−228.8
$c/a = 2.05$	—	—	—	—	4.24	8.90	218	−230.0
				ϵ-Ti_2C				
GGA/FLAPW	5.11	3.17	197	−184.7	5.10	3.20	193	−185.5
LDA/FLAPW [27]	5.03	3.09	—	−243.0	—	—	—	—
				TiC + Ti (segregation)				
GGA/FLAPW	—	—	—	−152.0	—	—	—	—
LDA/FLAPW [27]	—	—	—	−186.3	—	—	—	—

[a] Hex. α-Ti_2C.

atoms exceed those of the GGA/VASP calculation by 1.3% to 2.3%, and the FLAPW formation energies are also somewhat lower than the VASP results.

These differences can possibly be attributed to the taking over of a rather small value for the Ti muffin-tin radius from former calculations. Theoretically, the results of a converged FLAPW calculation should be independent of the muffin-tin radii. However, for a small Ti

Table 3. Transformation energies from trigonal to cubic Ti_2C in kJ mol^{-1}: (a) unrelaxed $R\bar{3}m$-Ti_2C (optimized c/a) to unrelaxed $Fd3m$-Ti_2C; (b) relaxed $R\bar{3}m$-Ti_2C (optimized c/a) to relaxed $Fd3m$-Ti_2C.

Method	(a)	(b)
GGA/FLAPW	3.2	−5.0
LDA/VASP [38]	—	−0.9
GGA/VASP [38]	—	−2.2

muffin-tin radius the Ti 3p wavefunctions partly extend into the interstitial and are thus not well described as core states. In this case, also the corresponding corrections provided by the FLAPW code might not be sufficient.

Compared to experiment, the lattice parameters of the present GGA/FLAPW calculation deviate by +2.3% (lattice parameter a) and −0.9% (lattice parameter c) for $R\bar{3}m$-Ti_2C and +2% (lattice parameter a) for $Fd3m$-Ti_2C. As quite often for GGA calculations, binding seems to be underestimated, which also shows up in a lower value for the bulk modulus of $Fd3m$-Ti_2C. In contrast to this behaviour, all referenced calculations with LDA exchange show the typical overbinding effect with lower values for the lattice parameters and higher values of the bulk modulus compared to experiment.

If the c/a ratio is optimized for fictitious δ'-Ti_2C with unrelaxed Ti atoms, the minimum of the total energy lies at $c/a = 2.0$, corresponding to an fcc lattice with the vacancies at the positions of the δ'-structure ('ordered Ti_2C'). For relaxed Ti atoms, an optimized c/a ratio of 2.1 is found. The energy gain by relaxation is quite large for δ'-Ti_2C with either $c/a = 2.0$ or especially $c/a = 2.1$, but it is nevertheless not sufficient to make the fictitious δ'-phase more stable than the other Ti_2C phases with relaxed Ti atoms. In the former FLAPW calculation [27], the fictitious phases δ'-Ti_2C and ϵ-Ti_2C were found to be—in disagreement with the experimental situation—more stable than $Fd3m$-Ti_2C and (in the case of fictitious ϵ-Ti_2C) also $R\bar{3}m$-Ti_2C.

From the present calculation, fictitious ϵ-Ti_2C—although not found by experiment—should be thermodynamically as stable as $R\bar{3}m$-Ti_2C in its most stable geometry. For kinetic reasons, however, its formation is highly improbable, as even the corresponding nitride, ϵ-Ti_2N, cannot be formed directly but only from a precursor phase, namely metastable δ'-Ti_2N [35]. Considering the low stability of δ'-Ti_2C, this mechanism of formation is most unlikely to occur for the carbide.

The experimental formation energies at 298 K (ΔH^{B}_{298}) for unspecified hexagonal α-Ti_2C are taken from a recent thermodynamic description of the Ti–C system [39], where different experimental and calculated values for ΔH^{B}_{298} are summarized and evaluated. From table 2 it is obvious that all Ti_2C phases have a higher formation energy than the system (TiC + Ti) and can thus be supposed to be stable against segregation into TiC and Ti.

Table 3 shows the calculated transformation energies from cubic $Fd3m$-Ti_2C to trigonal $R\bar{3}m$-Ti_2C with unrelaxed and relaxed Ti atoms. Whereas the former FLAPW-LDA calculation [27] predicted the trigonal phase to be more stable than the cubic phase by more than 30 kJ mol^{-1}, the present calculation furnishes a different result. Without relaxation of the Ti atoms, the trigonal phase in its equilibrium geometry is still more stable by 3.2 kJ mol^{-1} than the cubic phase, whereas, owing to the much larger relaxation energy of the cubic phase, relaxed $Fd3m$-Ti_2C is now more stable by 5.0 kJ mol^{-1} than relaxed trigonal $R\bar{3}m$-Ti_2C.

In the VASP calculations [38], relaxed cubic $Fd3m$-Ti_2C is also found to be the most stable phase, but with a smaller energy difference from the trigonal phase compared to the FLAPW value.

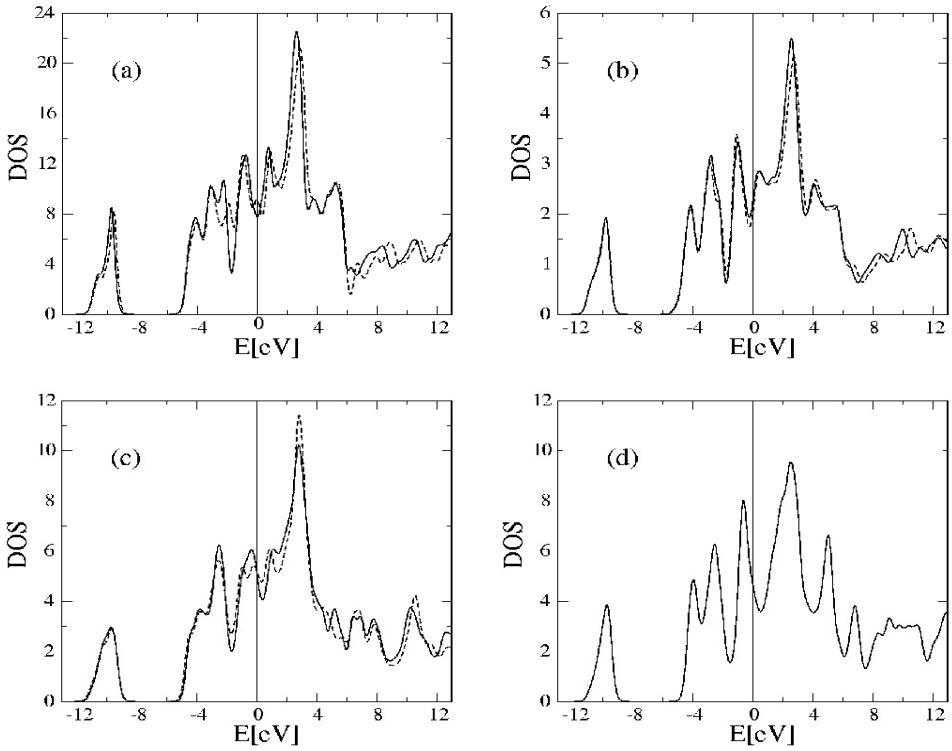

Figure 3. GGA-PW91 densities of states of relaxed (full line) and unrelaxed (dashed line) (a) $Fd3m$-Ti_2C; (b) $R\bar{3}m$-Ti_2C; (c) δ'-Ti_2C; (d) ϵ-Ti_2C. The densities of states are plotted in units of states of both spin directions per electronvolt and unit cell (containing for $R\bar{3}m$-Ti_2C one, for δ'-Ti_2C and ϵ-Ti_2C two, and for $Fd3m$-Ti_2C four formula units of Ti_2C per unit cell).

3.1.2. Densities of states. Figure 3 shows the GGA densities of states (DOS) of the four Ti_2C phases considered here with relaxed as well as with unrelaxed Ti atoms. Further, in figure 4 their partial local C s, C p and Ti d densities of states are presented.

The lowest DOS peak at approximately −10 eV ('s band') can be ascribed to C 2s states interacting to a certain extent with Ti 3d states. After a gap of 2.4–2.8 eV there comes a peak with two or three subpeaks ('p band') originating from C 2p states interacting with Ti 3d states. The p band subpeaks are most pronounced for $R\bar{3}m$- and ϵ-Ti_2C.

After a sharp minimum follows the 'd band', originating mainly from Ti d states. The lowest d band peak situated below E_F can be ascribed to Ti 3d states interacting across the C vacancies and thus lowered in energy compared to the other Ti 3d states.

A detailed analysis of the states contributing to the different DOS peaks can be found in [27].

The main difference between the densities of states of the four phases lies in the position of the Fermi level. For relaxed $Fd3m$-Ti_2C and for $R\bar{3}m$-Ti_2C, it lies in a most favourable position, namely in the DOS minimum separating the lowest d band peak from the rest of the d band. For the fictitious phases δ'- and ϵ-Ti_2C, it is situated—much less favourably—in this peak.

For unrelaxed $Fd3m$-Ti_2C, the Fermi level also lies in a small DOS peak, and the p and d bands are not separated by a pronounced DOS minimum. However, relaxation leads to

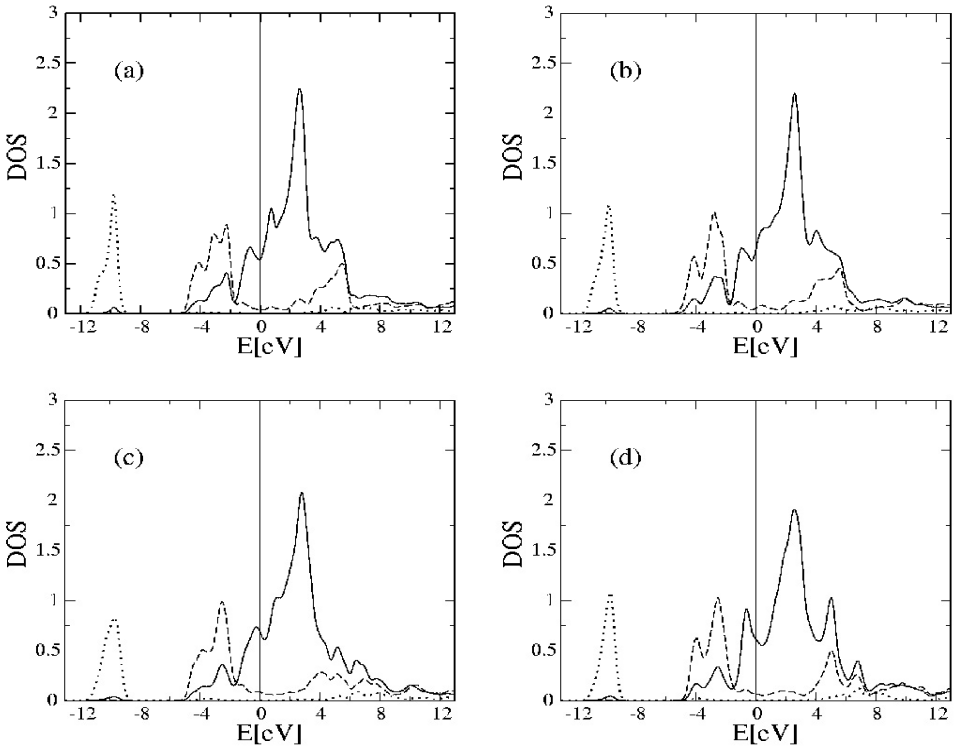

Figure 4. GGA-PW91 local Ti d (full line), C p (dashed line) and C s (dotted line) partial densities of states of relaxed (a) $Fd3m$-Ti_2C; (b) $R\bar{3}m$-Ti_2C; (c) δ'-Ti_2C; (d) ϵ-Ti_2C. The local densities of states are plotted in units of states of both spin directions per electronvolt and atom.

significant changes of the DOS which can serve as an explanation for the considerable energy gain by relaxation of the Ti atoms for this structure. For relaxed $Fd3m$-Ti_2C, the states in the C p band describing C p–Ti d bonds are lowered in energy, the small DOS peak at the Fermi level disappears and the Fermi energy now lies in the newly formed energy minimum.

Relaxation effects are also considerable for the DOS of fictitious δ'-Ti_2C. Only after relaxation of the Ti atoms, the Ti d states at the bottom of the d band peak are separated by a distinct minimum from the rest of the d band.

Much smaller are the effects of relaxation on the DOS of $R\bar{3}m$-Ti_2C. For ϵ-Ti_2C, they are even too small to be visible in the DOS plot.

3.2. Ti_2N phases

3.2.1. Energetics. Figure 5 shows the Birch fits for fictitious unrelaxed and relaxed $Fd3m$-Ti_2N and $R\bar{3}m$-Ti_2N, for stable ϵ-Ti_2N and for unrelaxed and relaxed δ'-Ti_2N with a c/a ratio of 2.0 (corresponding to 'ordered' Ti_2N) and with the equilibrium c/a ratio of 2.16 for relaxed δ'-Ti_2N, respectively. The plots are again based on GGA band-structure calculations with the PW91 exchange–correlation potential [32].

In agreement with experiment [12–14] and with previous LDA-FLAPW band-structure calculations [16], ϵ-Ti_2N is found to be the most stable phase at the equilibrium volume of 38.6 $Å^3$. For this compound, the Ti atoms do not relax from their experimental positions and the equilibrium c/a ratio coincides with the experimental value.

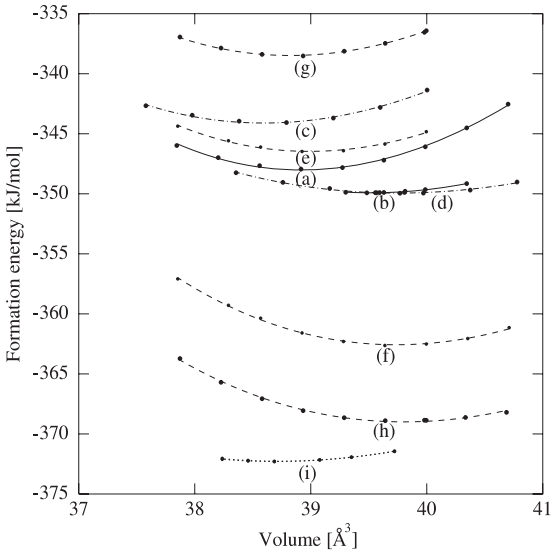

Figure 5. Total energies (in kJ mol^{-1} of Ti_2N) of various ordered titanium nitride phases of composition Ti_2N resulting from GGA-PW91 band-structure calculations: (a) unrelaxed $Fd3m$-Ti_2N; (b) relaxed $Fd3m$-Ti_2N; (c) unrelaxed $R\bar{3}m$-Ti_2N, $c/a = 4.7720$; (d) relaxed $R\bar{3}m$-Ti_2N, $c/a = 4.7233$; (e) unrelaxed δ'-Ti_2N, $c/a = 2.0$; (f) relaxed δ'-Ti_2N, $c/a = 2.0$; (g) unrelaxed δ'-Ti_2N, $c/a = 2.16$; (h) relaxed δ'-Ti_2N, optimized c/a (2.16); (i) ϵ-Ti_2N.

Table 4. Relaxation of Ti atoms in $Fd3m$-, $R\bar{3}m$-and δ'-Ti_2N.

Method	Relaxation (Å)	Relaxation energy (kJ mol^{-1} of Ti_2N)	Volume increase (%)
	$Fd3m$-Ti_2N		
GGA/FLAPW	0.014	−2.0	1.6
	$R\bar{3}m$-Ti_2N		
GGA/FLAPW			
$c/a = 4.7233$	0.011	−5.9	3.0
	δ'-Ti_2N		
GGA/FLAPW			
$c/a = 2.0$	0.085	−16.1	1.9
$c/a = 2.16$	0.144	−30.3	2.5
LDA-FLAPW [16]			
$c/a = 2.0$	0.095	−15.3	—
$c/a = 2.1126$	0.140	−28.8	—
exp. [11]			
$c/a = 2.1174$	0.123	—	—

For all other phases, table 4 shows the Ti relaxations and relaxation energies together with the increase of the equilibrium volume if the Ti atoms are allowed to relax. For $Fd3m$-Ti_2N and δ'-Ti_2N, the relaxations of the Ti atoms again refer to the ideal positions of the fcc sublattice, for ϵ-Ti_2N to their experimental atomic coordinates and for fictitious $R\bar{3}m$-Ti_2N to the experimental coordinates of the Ti atoms in $R\bar{3}m$-Ti_2C.

Table 5. Equilibrium lattice parameters (in Å), compression moduli B_0 (in GPa) and formation energies (in kJ mol^{-1}) of various ordered titanium nitride phases with unrelaxed and relaxed Ti atoms. The calculated values are valid for 0 K.

	Unrelaxed Ti				Relaxed Ti			
Method	a	c	B_0	E_{form}	a	c	B_0	E_{form}
				$Fd3m$-Ti_2N				
GGA/FLAPW	8.54	—	236	−348.1	8.58	—	153	−350.1
				$R\bar{3}m$-Ti_2N				
GGA/FLAPW								
$c/a = 4.7720$	3.04	14.51	182	−344.2	—	—	—	
$c/a = 4.7233$	—	—	—	—	3.08	14.55	111	−350.1
				δ'-Ti_2N				
GGA/FLAPW								
$c/a = 2.0$	4.27	8.54	208	−346.5	4.30	8.60	192	−362.7
$c/a = 2.16$	4.16	8.99	262	−338.7	4.19	9.05	168	−368.2
LDA/FLAPW [16]								
$c/a = 2.1126$	4.12	8.72	232	—	—	—	—	—
exp. [11]								
$c/a = 2.1174$	—	—	—	—	4.15	8.79	—	—
				ϵ-Ti_2N				
GGA/FLAPW	5.01	3.08	108	−372.1	5.01	3.08	122	−372.1
LDA/FLAPW [16]	4.91	3.02	231	—	—	—	—	—
exp. [15]	—	—	—	—	4.94	3.04	—	—
				Ordered Ti_2N				
LDA/FLAPW [36]	4.13	—	233	—	—	—	—	—
				TiN + Ti (segregation)				
GGA/FLAPW	—	—	—	−322.1	—	—	—	—

Among the unrelaxed structures, the least stable phase is again unrelaxed δ'-Ti_2N with $c/a = 2.16$. However, the energy difference from the other unrelaxed phases is much smaller than for the carbide, and the large energy gain of 30.3 kJ mol^{-1} of atoms by relaxation makes relaxed δ'-Ti_2N with $c/a = 2.16$ more stable than all the other phases apart from ϵ-Ti_2N. Moreover, the energy difference from ϵ-Ti_2N is rather small (3.2 kJ mol^{-1} of Ti_2N), and from figure 5 it can be deduced that at larger volumes the δ'-phase could even become the most stable phase.

Unrelaxed $Fd3m$-Ti_2N is more stable than unrelaxed δ'-Ti_2N and $R\bar{3}m$-Ti_2N. However, and in contrast to the carbide, the energy gain by relaxation is rather small for $Fd3m$-Ti_2N (2.0 kJ mol^{-1} of Ti_2N). Therefore, relaxed $Fd3m$-Ti_2N is thermodynamically less stable than all the other phases with relaxed Ti atoms.

Table 5 shows the equilibrium geometries, bulk moduli and formation energies of the four Ti_2N phases and also the formation energy for the case of segregation ($Ti_2N \rightarrow TiN + Ti$). Again, all four ordered Ti_2N phases are stable against segregation.

The GGA/FLAPW equilibrium lattice parameters of ϵ-Ti_2N deviate by $+1.3\%$ from the experimental values, whereas the values resulting from a former LDA/FLAPW calculation [16] are lower than experiment by -0.7%.

Table 6. Transformation energies from δ'-Ti_2N to ϵ-Ti_2N (in kJ mol^{-1} of Ti_2N). (a) Unrelaxed δ'-Ti_2N ($c/a = 2.0$) to ϵ-Ti_2N; (b) unrelaxed δ'-Ti_2N ($c/a = 2.16$) to ϵ-Ti_2N; (c) relaxed δ'-Ti_2N ($c/a = 2.0$) to ϵ-Ti_2N; (d) relaxed δ'-Ti_2N ($c/a = 2.16$) to ϵ-Ti_2N.

Method	(a)	(b)	(c)	(d)
GGA/FLAPW	−25.6	−33.5	−9.5	−3.2
LDA/FLAPW [16]	−32.5	−38.1	−17.4	−9.4

The lattice parameter a of relaxed δ'-Ti_2N (4.19 Å) is only 1% bigger than the experimental value of 4.15 Å [11]. However, because of the higher calculated equilibrium c/a ratio of 2.16 compared to the experimental c/a ratio of 2.1174 [11], the calculated lattice parameter c of this compound deviates by almost 3% from the experimental value.

Table 6 shows the transformation energies from unrelaxed and relaxed metastable δ'-Ti_2N to thermodynamically stable ϵ-Ti_2N resulting from the present GGA-FLAPW calculation and from the former LDA-FLAPW calculation [16]. In both calculations, transformation energies of more than −25 kJ mol^{-1} are found for unrelaxed δ'-Ti_2N, which are, however, much reduced by allowing the Ti atoms in δ'-Ti_2N to relax. In all cases, the GGA values lie below the LDA values.

3.2.2. Densities of states. Figure 6 shows the DOS of the four relaxed and unrelaxed Ti_2N phases and figure 7 their partial local N s and p and Ti d densities of states.

Nitrogen is more electronegative than carbon. Therefore, in the nitrides the non-metal s and p bands are narrower and situated at lower energies compared to the carbides, and the s–p gap is larger. Also, the p–d mixing in the p band is reduced, and the d band is now separated from the p band by a pseudogap.

Because of one additional valence electron per formula unit in the nitrides compared to the carbides, the Fermi level for ϵ-Ti_2N and δ'-Ti_2N moves to a favourable position in the minimum after the first d band peak, and for $Fd3m$-Ti_2N and $R\bar{3}m$-Ti_2N to a less favourable position in the small peak (shoulder) above this minimum.

The effects of the Ti-atom relaxation on the DOS of $R\bar{3}m$-Ti_2N and $Fd3m$-Ti_2N are small. In the case of δ'-Ti_2N, the stabilizing effect of the considerable Ti atom relaxation is also visible in the DOS. Relaxation shifts all occupied bonding states in the s, p and first d band peaks to lower energies and deepens the DOS minimum at the Fermi level. Also, the small peak at the bottom of the p band is more pronounced for relaxed than for unrelaxed δ'-Ti_2N.

3.3. Electron densities

The contour-line plots of the valence-electron densities in the (100) plane of relaxed $Fd3m$-Ti_2C, $Fd3m$-Ti_2N, δ'-Ti_2C and δ'-Ti_2N are presented in figures 8 and 9. For the nitride phases, the plots show—as expected—weaker Tid–C (N) p bonds and stronger d–d bonds between Ti atoms adjacent to the non-metal vacancies. Moreover, the additionally occupied d band states in the nitrides change the symmetry of the total valence-electron density around these Ti atoms from e_g-like for the carbides to t_{2g}-like for the nitrides.

If only the contributions to the valence-electron density of states with energies in the energy range of the p band are added up, one gets the so-called p band electron density. Analogously, the d band electron density only contains contributions from states in the occupied d band energy range. The partial electron-density plots show more clearly the bonding situation and are more suitable for demonstrating the influence of relaxation on chemical bonding than the total valence-electron density plots.

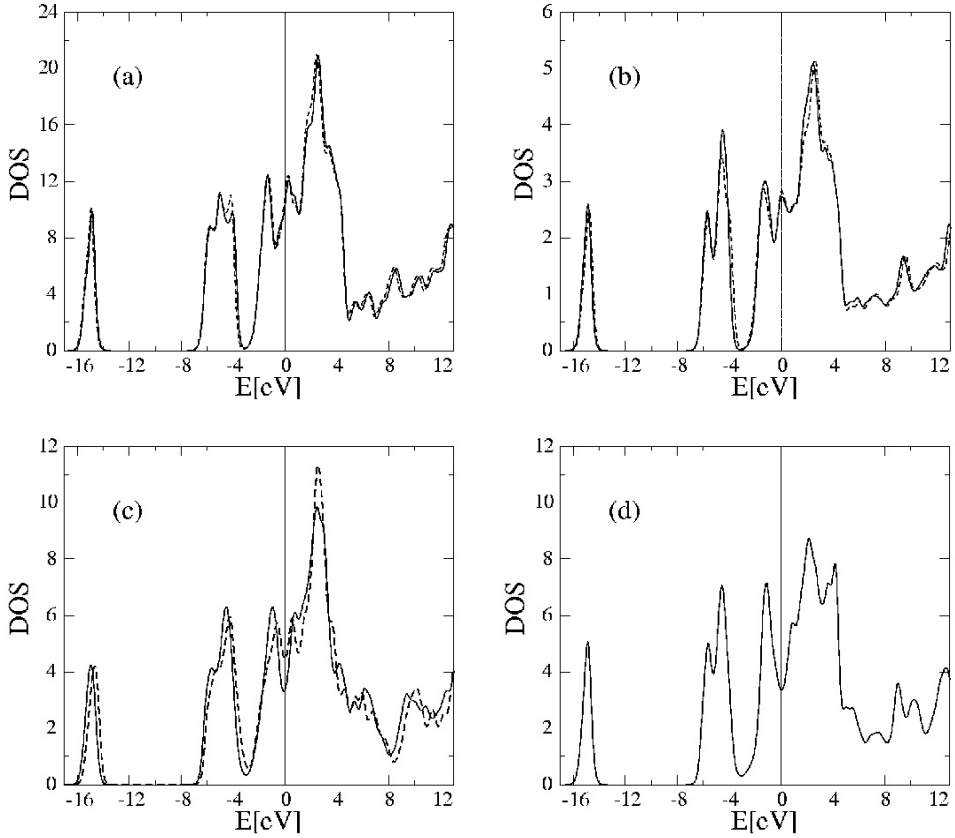

Figure 6. GGA-PW91 densities of states of relaxed (full line) and unrelaxed (dashed line) (a) $Fd3m$-Ti_2N; (b) $R\bar{3}m$-Ti_2N; (c) δ'-Ti_2N; (d) ϵ-Ti_2N. The densities of states are plotted in units of states of both spin directions per electronvolt and unit cell (containing for $R\bar{3}m$-Ti_2N one, for δ'-Ti_2N and ϵ-Ti_2N two and for $Fd3m$-Ti_2N four formula units of Ti_2N per unit cell).

Figures 10 and 11 thus present the contour-line plots in the (100) plane of the p and d band electron densities of unrelaxed and relaxed $Fd3m$-Ti_2C and $Fd3m$-Ti_2N; figures 12 and 13 show the p and d band electron-density plots in the (100) plane of unrelaxed δ'-Ti_2C and δ'-Ti_2N with $c/a = 2.0$, and of relaxed δ'-Ti_2C with $c/a = 2.1$ and δ'-Ti_2N with $c/a = 2.16$, respectively.

These p and d band electron density plots show that in all phases mainly Ti d states with e_g symmetry forming σ bonds with non-metal p states are present in the p band, whereas mainly Ti d states of t_{2g} symmetry forming Ti d–d bonds can be found in the d band energy range. Some octahedral d–d bonding between d states at Ti atoms adjacent to the vacancies is already present in the carbide phases but is found to a greater extent in the nitride phases. The d band electron density plots of the latter also show—especially for relaxed δ'-Ti_2N—d–d bonds between Ti d states adjacent to the non-metal atoms.

The most remarkable effects by relaxation which also explain the especially high relaxation energies in these phases are the strengthening of the C p–Ti d bonds in relaxed $Fd3m$-Ti_2C and the formation of d–d bonds between Ti atoms adjacent to the N atoms in relaxed δ'-Ti_2N with $c/a = 2.16$.

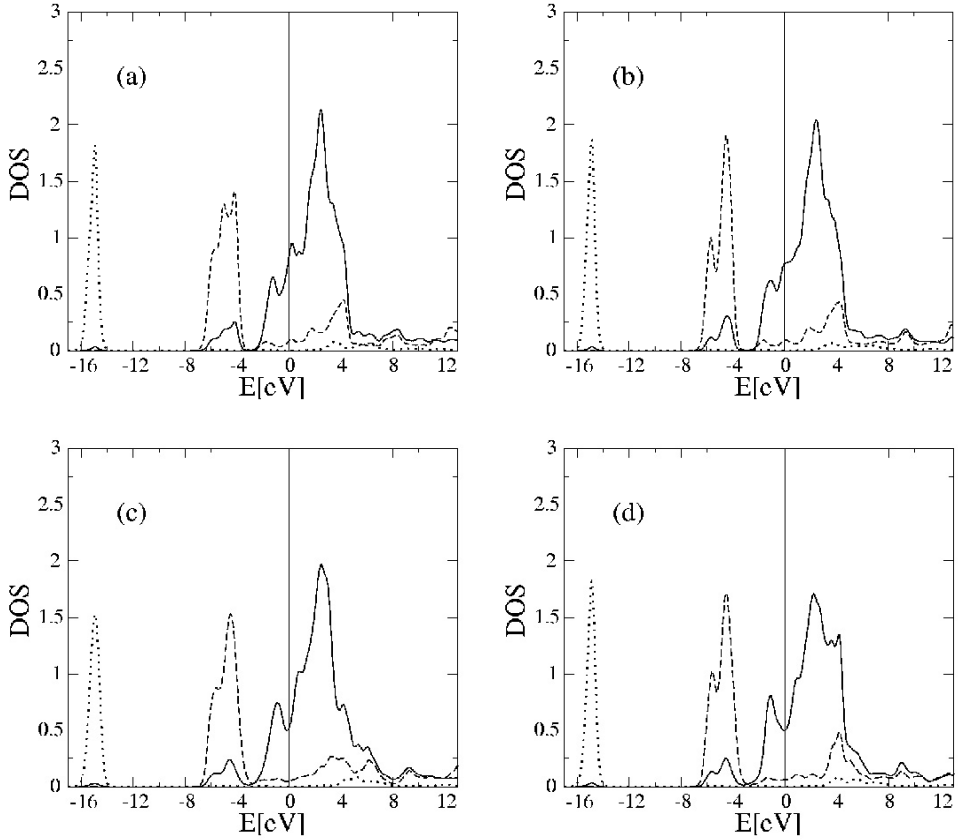

Figure 7. GGA-PW91 partial local Ti d (full line), N s (dotted line) and N p (dashed line) densities of states of relaxed (a) $Fd\bar{3}m$-Ti_2N; (b) $R\bar{3}m$-Ti_2N; (c) δ'-Ti_2N; (d) ϵ-Ti_2N. The local densities of states are plotted in units of states of both spin directions per electronvolt and atom.

Figures 14 and 15 present the contour-line plots in the (001) plane of the total valence-electron densities and the p band and the d band electron densities of ϵ-Ti_2C and ϵ-Ti_2N. The tetragonal antirutile structure consists of Ti_2X units aligned in parallel rows in the [110] direction in the basal plane. The [110] direction coincides with the local z axis.

The p band electron density contour plots (figures 15(a) and (b)) show the Ti and non-metal atoms in these units to be connected by strong p–d σ bonds between C (N) p and e_g-like Ti d states.

The d band electron density contour plots of ϵ-Ti_2C and ϵ-Ti_2N (figures 15(c) and (d)) reveal that in these phases Ti d states of both e_g and (to a lesser extent) t_{2g} symmetry are responsible for d–d bonding between Ti atoms belonging to parallel Ti_2X units. These d–d bonds are stronger in the nitride than in the carbide. Further, they are also more efficient in ϵ-Ti_2N than in the other nitride phases, thus explaining the high stability of ϵ-Ti_2N. Stronger bonds between Ti d states in ϵ-Ti_2N than in δ'-Ti_2N were also found in a former APW band structure calculation [41]. Also, covalent bond densities and bond overlap populations from first-principles DV-Xα cluster calculations [42] show the Ti–Ti bonds in ϵ-Ti_2N to be much stronger than in B1-TiN.

The contour-line plots in the (010) plane of the total valence-electron, p band and d band electron densities of $R\bar{3}m$-Ti_2C and $R\bar{3}m$-Ti_2N are presented in figures 16 and 17. The trigonal

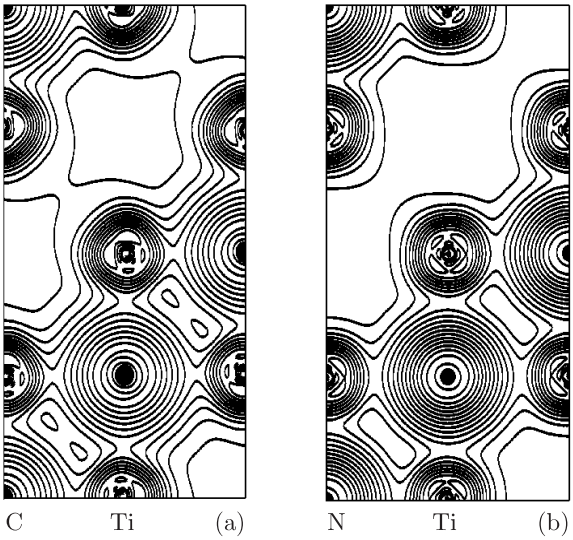

Figure 8. Contour lines in the (100) plane of the total valence-electron densities of (a) relaxed $Fd3m$-Ti_2C and (b) relaxed $Fd3m$-Ti_2N. A logarithmic grid of contour lines with $x_i = 2^{i/4}$ has been used.

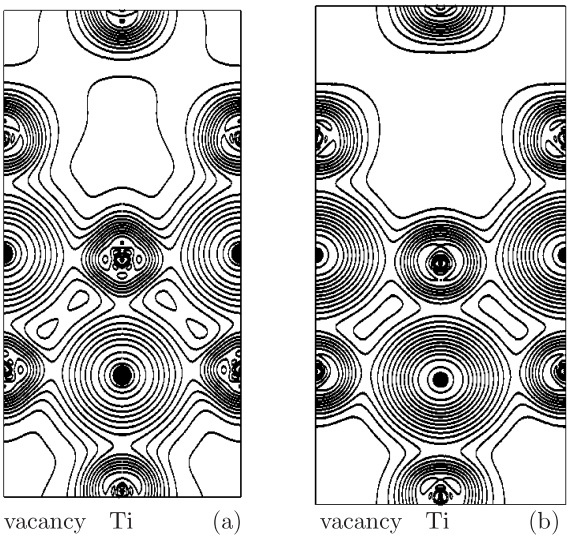

Figure 9. Contour lines in the (100) plane of the total valence-electron densities of (a) relaxed δ'-Ti_2C with $c/a = 2.1$ and (b) relaxed δ'-Ti_2N with $c/a = 2.16$. A logarithmic grid of contour lines has been used ($x_i = x_0 2^{i/4}$).

$R\bar{3}m$-structure consists of three-layer strings formed by parallel Ti_2X units. The p band electron density contour plots in figures 17(a) and (b) show the individual Ti_2X units to be held together by strong p–d σ bonds between non-metal p and e_g-like Ti d states. The latter also form d–d bonds with the nearest Ti atoms belonging to the next parallel Ti_2X unit within the same string. However, the Ti d–N p bonds in $R\bar{3}m$-Ti_2N are weaker and above all more ionic than the

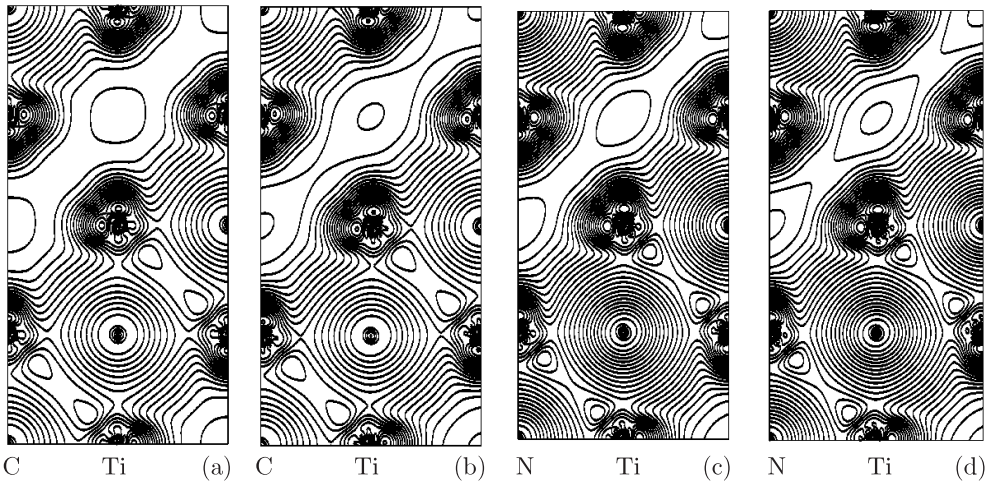

Figure 10. Contour lines in the (100) plane of the p band electron densities of unrelaxed (a) and relaxed (b) $Fd3m$-Ti_2C, and of unrelaxed (c) and relaxed (d) $Fd3m$-Ti_2N. A logarithmic grid of contour lines has been used ($x_i = x_0 2^{i/4}$).

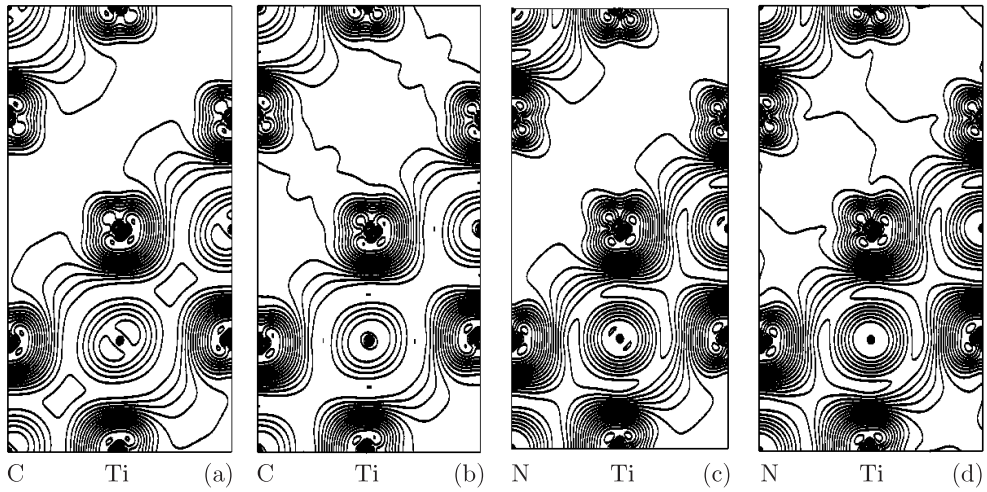

Figure 11. Contour lines in the (100) plane of the d band electron densities of unrelaxed (a) and relaxed (b) $Fd3m$-Ti_2C, and of unrelaxed (c) and relaxed (d) $Fd3m$-Ti_2N. A logarithmic grid of contour lines has been used ($x_i = x_0 2^{i/4}$).

C–Ti bonds in $R\bar{3}m$-Ti_2C. Therefore, less charge resides on the Ti atoms in $R\bar{3}m$-Ti_2N than in $R\bar{3}m$-Ti_2C, thus leading in the nitride also to weaker d–d bonds between the nearest Ti–Ti neighbours.

The d band electron density contour plots of $R\bar{3}m$-Ti_2C and $R\bar{3}m$-Ti_2N (figures 17(c) and (d)) show the t_{2g}-like Ti d states of these phases in the d band energy range to be involved in weak d–d bonding between Ti atoms of parallel Ti_2X units belonging to different strings, but also to be of an antibonding nature between nearest Ti neighbours within the same string.

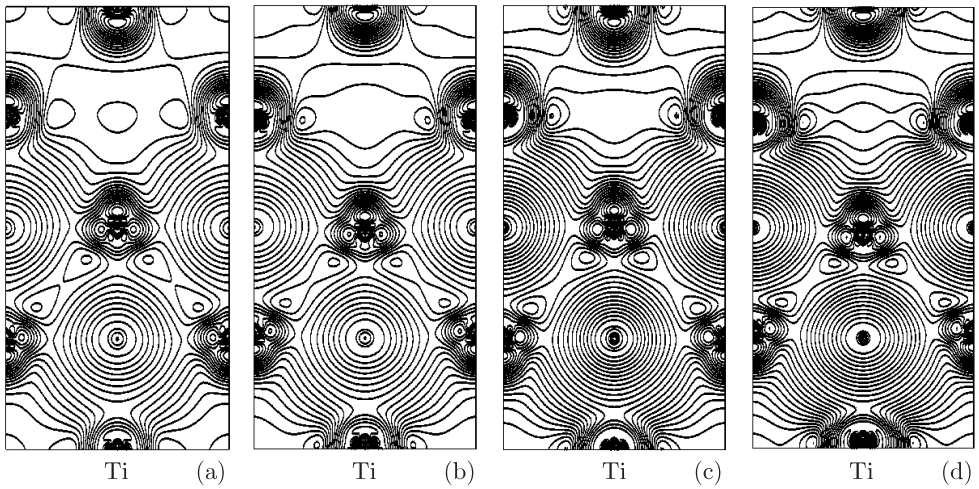

Figure 12. Contour lines in the (100) plane of the p band electron densities of unrelaxed δ'-Ti_2C with $c/a = 2.0$ (a), relaxed δ'-Ti_2C with $c/a = 2.1$ (b), unrelaxed δ'-Ti_2N with $c/a = 2.0$ (c) and relaxed δ'-Ti_2N with $c/a = 2.16$ (d). A logarithmic grid of contour lines has been used ($x_i = x_0 2^{i/4}$).

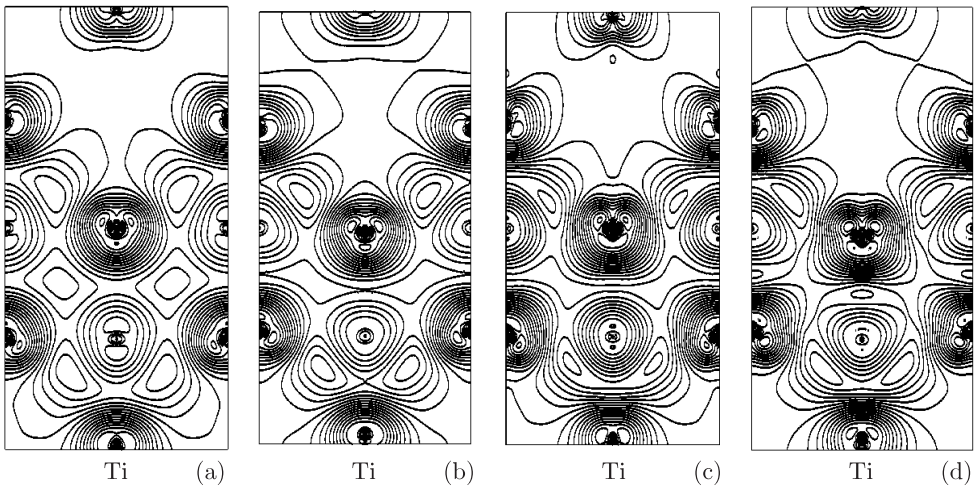

Figure 13. Contour lines in the (100) plane of the d band electron densities of unrelaxed δ'-Ti_2C with $c/a = 2.0$ (a), relaxed δ'-Ti_2C with $c/a = 2.1$ (b), unrelaxed δ'-Ti_2N with $c/a = 2.0$ (c) and relaxed δ'-Ti_2N with $c/a = 2.16$ (d). A logarithmic grid of contour lines has been used ($x_i = x_0 2^{i/4}$).

4. Discussion

The results of the present first-principles calculations for ordered $Ti_2C(N)$ phases of composition $TiC_{0.5}$ can be resumed as follows.

(i) In agreement with experimental findings for TiC_x samples of composition $TiC_{0.52}$ and $TiC_{0.54}$ [24] and also in agreement with a former first-principles FP-LMTO calculation [28] as well as a calculated phase diagram [29], cubic $Fd3m$-Ti_2C with relaxed Ti atoms is

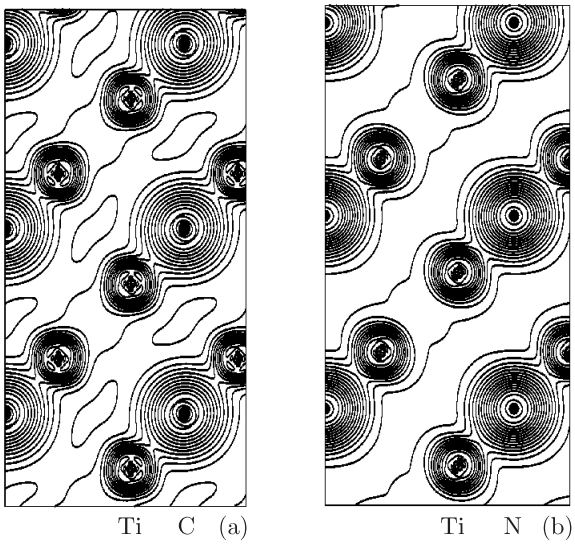

Figure 14. Contour lines in the (001) plane of the total valence-electron densities of relaxed ϵ-Ti_2C (a) and ϵ-Ti_2N (b). A logarithmic grid of contour lines has been used ($x_i = x_0 2^{i/4}$).

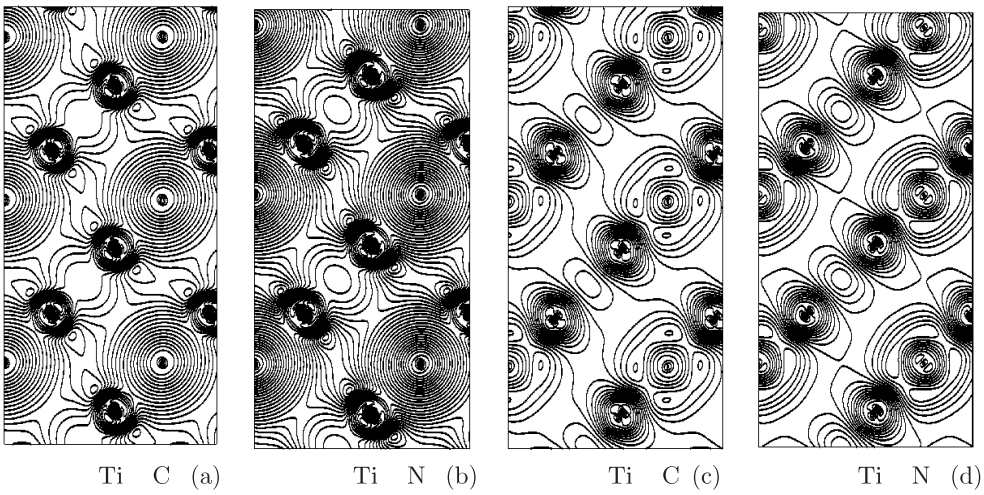

Figure 15. Contour lines in the (001) plane of the p band electron densities of relaxed ϵ-Ti_2C (a) and ϵ-Ti_2N (b) and of the d band electron densities of relaxed ϵ-Ti_2C (c) and ϵ-Ti_2N (d). A logarithmic grid of contour lines has been used ($x_i = x_0 2^{i/4}$).

found to be the most stable phase for the carbides and more stable by 5 kJ mol^{-1} than relaxed trigonal $R\bar{3}m$-Ti_2C.

However, if the Ti atoms are not relaxed the reverse is true, and unrelaxed $Fd3m$-Ti_2C is less stable by 3.2 kJ mol^{-1} than unrelaxed $R\bar{3}m$-Ti_2C. Hence, $Fd3m$-Ti_2C is stabilized with respect to $R\bar{3}m$-Ti_2C only by relaxation of the Ti atoms away from the vacancies towards the C atoms. This relaxation was found to be largest for ordered $TiC_{0.5}$ and decreased with increasing C content [28]. Therefore, the energy gain by relaxation for cubic $Fd3m$-Ti_2C should also decrease with increasing C content until—corresponding

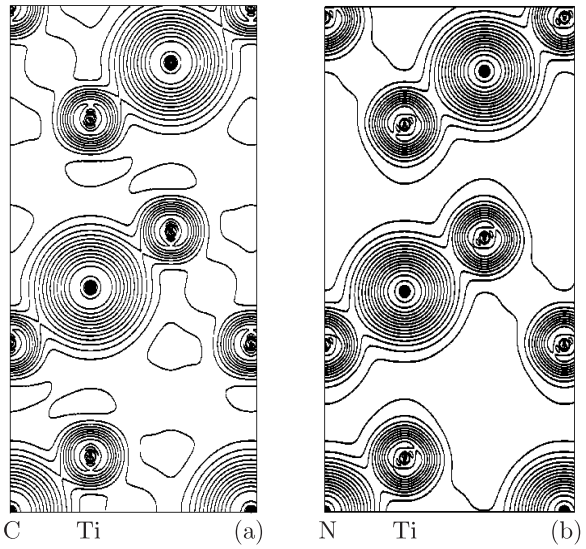

Figure 16. Contour lines in the (010) plane of the total valence-electron densities of relaxed $R\bar{3}m$-Ti_2C (a) and $R\bar{3}m$-Ti_2N (b). A logarithmic grid of contour lines has been used ($x_i = x_0 2^{i/4}$).

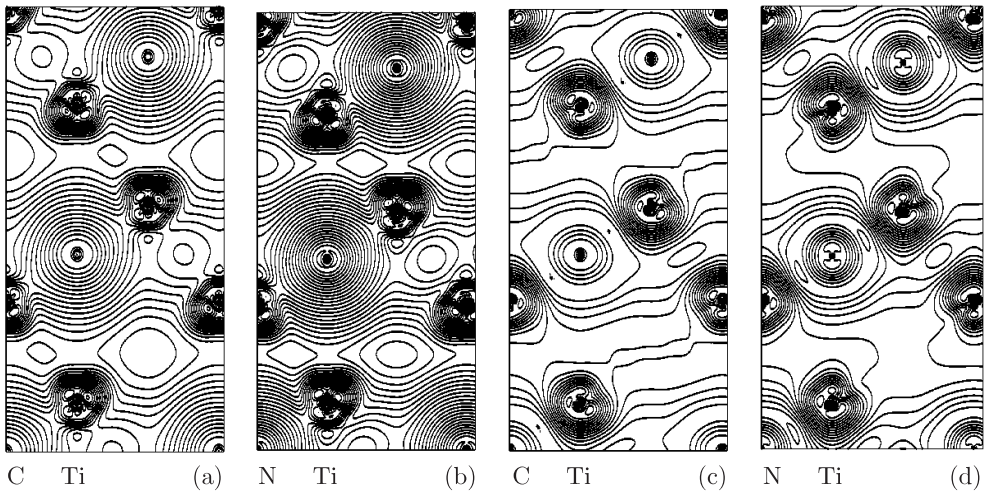

Figure 17. Contour lines in the (010) plane of the p band electron densities of relaxed $R\bar{3}m$-Ti_2C (a) and $R\bar{3}m$-Ti_2N (b), and of the d band electron densities of relaxed $R\bar{3}m$-Ti_2C (c) and $R\bar{3}m$-Ti_2N (d). A logarithmic grid of contour lines has been used ($x_i = x_0 2^{i/4}$).

to the calculated phase diagram [29]—the two phases are coexisting or the sequence of stability of the two phases is even reversed. Therefore, the present result, which predicts relaxed $Fd3m$-Ti_2C to be more stable than $R\bar{3}m$-Ti_2C for the exact composition $TiC_{0.5}$, is not incompatible with experiments, which find the reverse stability sequence for TiC_x samples of a composition near $TiC_{0.6}$ [21–24].

Both the $Fd3m$- and the δ'-structure with $c/a = 2$ can be constructed by positioning non-metal vacancies at specific lattice sites of the B1 structure. For the hemicarbides, unrelaxed

δ'-Ti_2C is less stable than unrelaxed $Fd3m$-Ti_2C by as much as 31.6 kJ mol^{-1}. Even the considerable energy gain by both relaxing the Ti atoms and increasing the c/a ratio from 2.0 to 2.1 is not sufficient to render its formation energy more negative than those of the other relaxed Ti_2C phases. Therefore, in agreement with all experimental findings, the δ-phase is not a stable phase for the carbides. Accordingly, the Fermi level for this fictitious phase is not situated in a DOS minimum as is indeed the case for the experimentally traced phases $R\bar{3}m$-Ti_2C and relaxed $Fd3m$-Ti_2C.

The present calculation predicts fictitious ϵ-Ti_2C to be of comparable stability with relaxed $R\bar{3}m$-Ti_2C. As already mentioned, however, its formation from the unstable precursor phase δ'-Ti2C is highly improbable.

(ii) For the heminitrides, unrelaxed δ'-Ti_2N is less stable than unrelaxed $Fd3m$-Ti_2N by only 3.6 kJ mol^{-1}. Further, cubic $Fd3m$-Ti_2N is almost not stabilized by relaxation whereas the relaxation energy of δ'-Ti_2N is even larger than for δ-Ti_2C. Hence, relaxed $Fd3m$-Ti_2N (and also relaxed $R\bar{3}m$-Ti_2N) are less stable by 38.1 kJ mol^{-1} than relaxed δ'-Ti_2N with the optimized c/a ratio of 2.16.

In agreement with experiment [15] and with previous calculations [16], tetragonal ϵ-Ti_2N is found to be the most stable heminitride phase. However, the energy difference from relaxed, tetragonally distorted δ'-Ti_2N with the optimized c/a ratio of 2.16 is quite small (3.3 kJ mol^{-1}).

δ'-Ti_2N is experimentally found to be the metastable precursor phase for ϵ-Ti_2N whose direct formation from substoichiometric TiN_x is kinetically hindered [35]. Accordingly, for the nitrides only the Fermi levels of δ'-Ti_2N and ϵ-Ti_2N lie in a DOS minimum.

(iii) One explanation for the different relative stabilities of the $Fd3m$- and the δ'-phase for carbides and nitrides is based on the different effects of Ti-atom relaxation on the chemical bonds in these phases, which are visualized in the present work by electron-density contour plots.

Generally speaking, the reduced number of Ti d–C (N) p bonds in non-stoichiometric carbides and nitrides with an underlying B1 structure is at least partially compensated by octahedral bonding involving the 3d states at the Ti atoms octahedrally surrounding the vacancies, which is found to a certain extent in the carbides but more so in the nitrides. Further, the relaxation of the metal towards the non-metal atoms (in x-, y- and z-directions for the $Fd3m$-structure; merely in the z-direction for the δ'-structure) reduces the nearest-neighbour Ti–C (N) distance and leads to a strengthening of the remaining Ti–non-metal bonds. Simultaneously, however, this relaxation weakens the d–d bonds between the Ti atoms adjacent to the vacancies.

Thus, $Fd3m$-Ti_2N is almost not stabilized by relaxation because in this compound the stabilizing effect on the Ti–non-metal bonds is compensated by the destabilizing effect on the Ti–Ti d–d bonds. For $Fd3m$-Ti_2C with fewer occupied octahedral bonding states and much stronger covalent C p–Ti d bonds, the positive effects of relaxation predominate. This leads to a large relaxation energy, which makes relaxed $Fd3m$-Ti_2C more stable than all the other carbide phases.

For the δ'-structure, the overall effect of relaxation and tetragonal distortion increasing the c/a ratio at constant volume does not only lead to a shorter nearest-neighbour Ti–C (N) distance strengthening the Ti d–C (N) p bonds, but also to a shorter distance between the Ti atoms next to the C (N) atoms, which enables stronger d–d bonds between these Ti atoms. However, the corresponding electronic states are not occupied in the carbide, and these stronger bonds are therefore only visible in the d band electron density plots of relaxed δ'-Ti_2N. For the same reason, the relaxation energy of δ'-Ti_2N exceeds the relaxation energy of δ'-Ti_2C.

(iv) The transformation of δ'-Ti_2N to ϵ-Ti_2N leads to even stronger Ti–Ti d–d bonds making ϵ-Ti_2N the most stable heminitride phase. In ϵ-Ti_2C, Ti–Ti d–d bonding is less pronounced because in the carbide fewer of the responsible d band states are occupied.
Trigonal $R\bar{3}m$-Ti_2C is mainly stabilized by strong covalent nearest-neighbour C–Ti p–d bonds involving states in the p band energy range which are also responsible for some interlayer d–d bonding between Ti atoms of the same string. In $R\bar{3}m$-Ti_2N, the N–Ti p–d bonds are not only weaker but also more ionic than in the carbide, leading for the nitride also to weaker Ti–Ti d–d bonds between nearest Ti neighbours in the same string. Also, the additional t_{2g}-like occupied Ti d states in the nitride—weakly bonding with respect to the Ti atoms in the next string but antibonding with respect to the nearest Ti atoms within the same string—cannot contribute much to its stability. This could explain why $R\bar{3}m$-Ti_2N is the least stable of all the investigated nitride phases.

Acknowledgments

All calculations were performed at the Schrödinger III Linux cluster of the Vienna University Computer Centre. Special thanks are due to W Wolf for performing the VASP calculations for relaxed $Fd3m$-Ti_2C and $R\bar{3}m$-Ti_2C as well as for stimulating discussions, and to P Herzig for carefully proof-reading the manuscript.

References

[1] Freer R (ed) 1990 *The Physics and Chemistry of Carbides, Nitrides and Borides* (*NATO ASI Series E* vol 185) (Dordrecht: Kluwer)
[2] Toth L E 1971 *Transition Metal Carbides and Nitrides* (New York: Academic)
[3] Gusev A I and Rempel A A 1997 *Phys. Status Solidi* a **163** 273–303
[4] Ehrlich P 1953 *Z. Anorg. Chem.* **259** 1–43
[5] Wriedt H A and Murray J L 1987 *Bull. Alloy Phase Diagrams* **8** 378–88
[6] Poulek V, Musil J, Valvoda V and Cerny R 1988 *J. Phys. D: Appl. Phys.* **21** 1657–8
[7] de Novion C H, Beuneu B, Priem T, Lorenzelli N and Finel A 1990 *The Physics and Chemistry of Carbides, Nitrides and Borides* (*NATO ASI Series E* vol 185) (Dordrecht: Kluwer) pp 329–55
[8] Gusev A I and Rempel A A 1993 *Phys. Status Solidi* a **135** 15–58
[9] Lobier G and Marcon J P 1969 *C. R. Acad. Sci., Paris* C **268** 1132–5
[10] Nagakura S and Kusunoki T 1977 *J. Appl. Crystallogr.* **10** 52–6
[11] Christensen A N, Alamo A and Landesman J P 1985 *Acta Crystallogr.* C **41** 1009–11
[12] Zeng K and Schmid-Fetzer R 1996 *Z. Metallk.* **87** 540–54
[13] Lengauer W and Ettmayer P 1987 *High Temp.—High Pressures* **19** 673–6
[14] Etchessahar E, Sohn Y-U, Harmelin M and Debuigne J 1991 *J. Less-Common Met.* **167** 261–81
[15] Holmberg B 1962 *Acta Chem. Scand.* **16** 1255–61
[16] Eibler R 1998 *J. Phys.: Condens. Matter* **10** 10223–40
[17] Goretzki H 1967 *Phys. Status Solidi* **20** K141–3
[18] Moisy-Maurice V, Lorenzelli N, de Novion C H and Convert P 1982 *Acta Metall.* **30** 1769–79
[19] Parthé E and Yvon K 1970 *Acta Crystallogr.* B **26** 153–63
[20] de Novion C H and Landesmann J P 1985 *Pure Appl. Chem.* **57** 1391–402
[21] Tsurekawa S and Yoshinaga H 1992 *J. Japan Inst. Met.* **56** 133–41
[22] Em V T and Tashmetov M Yu 1996 *Phys. Status Solidi* b **198** 571–5
[23] Tashmetov M Yu, Em V T, Lee C H, Shim H S, Choi Y N and Lee J S 2002 *Physica* B **311** 318–25
[24] Lipatnikov V N, Kottar A, Zueva V and Gusev A I 1998 *Phys. Solid State* **40** 1211–8
[25] Wanjara P, Drew R A L, Root J and Yue S 2000 *Acta Mater.* **48** 1443–50
[26] Massalski T B, Murray J L and Bennet L H (ed) 1986 *Binary Alloy Phase Diagrams* (Murray Park, OH: ASM)
Jonsson S 1996 *Z. Metallk.* **87** 703–12
[27] Eibler R 2002 *J. Phys.: Condens. Matter* **14** 4425–44
[28] Hugosson H W, Korzhavyi P, Jansson U, Johansson B and Eriksson O 2001 *Phys. Rev.* B **63** 165116

[29] Korzhavyi P A, Pourovskii L V, Hugosson H W, Ruban A V and Johansson B 2002 *Phys. Rev. Lett.* **88** 015505
[30] Wimmer E, Krakauer H, Weinert M and Freeman A J 1981 *Phys. Rev.* B **24** 864–75
Jansen H and Freeman A J 1984 *Phys. Rev.* B **30** 561–9
[31] www.uwm.edu/∼weinert/flair.html
[32] Perdew J P, Chevary J A, Vosko S H, Jackson K A, Pederson M R, Singh D J and Fiolhais C 1992 *Phys. Rev.* B **46** 6671–87
[33] Birch F 1978 *J. Geophys. Res.* **83** 1257–68
[34] Hedin L and Lundqvist S 1972 *J. Physique Coll.* **33** 73–81
[35] Zhou X, Dong H K, Li H D and Liu B X 1988 *J. Appl. Phys.* **63** 4942–5
[36] Dridi Z, Bouhafs B, Ruterana P and Aourag H 2002 *J. Phys.: Condens. Matter* **14** 10237–49
[37] Guemmaz M, Mosser A, Ahujab R and Johansson B 1999 *Solid State Commun.* **110** 299–303
[38] Wolf W 2005 personal communication
[39] Frisk K 2003 *Calphad* **27** 367–73
[40] Fernández Guillermet A and Grimvall G 1992 *J. Phys. Chem. Solids* **53** 105–25
[41] Eibler R 1993 *J. Phys.: Condens. Matter* **5** 5261–76
[42] Mizumo M, Tanaka I and Adachi H 1999 *Phys. Rev.* B **59** 15033–47